PROCEEDINGS, Thirty-Third Workshop on Geothermal Reservoir Engineering
Stanford University, Stanford, California, January 28-30, 2008
SGP-TR-185

OPTIMIZATION OF GEOTHERMAL WELL STIMULATION DESIGN USING A GEOMECHANICAL RESERVOIR SIMULATOR

Keita Yoshioka[1], Bulent Izgec[1], and Riza Pasikki[2]

1. Chevron Energy Technology Company, Houston TX 77002, USA
2. Chevron Geothermal Salak, Jakarta 10270, Indonesia
e-mail: yoshk@chevron.com

ABSTRACT

Conventional geothermal applications are limited to those with sufficient temperature, thermal gradient, and permeability. If these applications could be expanded to those with low or zero permeability, tremendous energy resources would suddenly be available. Thermal fracturing techniques are being looked at as potential methods of commercializing these types of reservoirs.

One drawback of using thermal fracturing techniques is the complexity of the rock/fluid interactions and the difficulty in modeling them to get reasonable treatment designs. A major challenge involves modeling both conductive and convective heat transfer in a matrix, and the stresses impacted by the heat transfer and the fluid leak-off (pore pressure effect on stress). Since these effects are all inter-woven, they have to be coupled in order to get appropriate fluid injection rates, pumping times, and injection fluid temperature in a reservoir with uncertain properties (permeability, composition, and mechanical properties).

This paper shows treatment designs resulting from a recently developed GeoMechanical Reservoir Simulator (GMRS®*), which predicts heat and mass transfer, thermo-hydro-mechanical fracture opening and dilatancy, and productivity or injectivity enhancement. We also demonstrate that injector well performance can be evaluated real-time by a reformulated Hall integral and its derivative for a geothermal reservoir. GMRS

INTRODUCTION

Geothermal reservoirs differ significantly from their hydrocarbon counterparts and so do their remedial treatments. Typically these reservoirs are naturally fractured volcanic materials with varying mineralogy found over a wide temperature range. Zones with low permeability do not contribute enough water/steam to provide efficient recovery of heat from these reservoirs. The low permeability could either be naturally occurring or be caused by damages occurring during drilling and/or production phases. Permeability in these zones can be enhanced through methods of well stimulation such as acidizing and high-rate water injection. Acid stimulations have improved performances of six sub-commercial wells in the Salak geothermal field, which experienced formation damage problem, turning them into productive wells (Pasikki and Gilmore, 2006; Mahajan *et al*., 2006).

In the meantime, three massive water injection stimulation treatments have also been conducted on four wells with naturally low permeability characteristics. These stimulations included injection of 2.5 billion pounds of water and successfully increased well injectivity by more than 100%. Unlike hydrocarbon reservoirs, geothermal reservoir boundaries are somewhat vague. Therefore, new wells often encounter low or even zero permeability formations and need to be stimulated to provide adequate rates. In many scenarios, injecting massive amounts of water has been successful in stimulating existing and/or new fractures (Smith et al., 1975; Kappelmeyer, and Jung, 1987; Tenma *et al.*, 2003).

Fracture propagation in volcanic reservoirs tends to be caused by dilating existing fractures while tensile failure is the most common mechanism in sedimentary reservoirs. In this paper, we infer how a single fracture will be dilated from long term cold water injection under various operating schemes by utilizing a conceptual sector model. We will also address how fracture dilations can be diagnosed using reformulated Hall plots (Izgec and Kabir, 2007).

GMRS is a registered trademark of Chevron

REFORMULATED HALL PLOT

The injector well undergoes two distinct processes that alternate over its life to create the sustained injectivity. As solids are deposited in the fracture, the effective permeability of the exposed reservoir is gradually reduced. The plugging process continues until a critical pressure value is reached, which re-fractures the formation or extends/propagates the plugged fracture. Real–time assessment of fracture conductivity and associated surrounding formation damage is an essential step for maximizing and maintaining injector well performance.

A modified Hall plot and its derivative, an approach recently introduced, is utilized to monitor injectivity in a geothermal reservoir. As opposed to generating a single curve, this methodology consists of comparing and contrasting two curves for obtaining definitive clues. The derivative goes below the Hall integral curve during fracturing and rides above it when the plugging occurs. These two curves trace the same path in matrix-dominated flow. The derivative curve can be obtained either analytically or numerically. The analytical derivative is

$$D_{HI} = \alpha_1 W_i \left\{ \ln(r_e / r_w) + s^* \right\} \qquad (1)$$

where

$$\alpha_1 = \frac{141.2 B \mu}{kh} \qquad (2)$$

The mathematical derivation of the analytic derivative and calculations of pseudo skin (s^*) are provided elsewhere (Izgec and Kabir, 2007). The numeric derivative is simply:

$$D_{HI} = \frac{\mathrm{d}\int \left(p_{wf} - p_e\right) dt}{\mathrm{d}\ln(W_i)} = \frac{\int \left(p_{wf} - p_e\right)^{n+1} dt - \int \left(p_{wf} - p_e\right)^{n} dt}{\ln(W_i)^{n+1} - \ln(W_i)^{n}} \qquad (3)$$

The disagreement between analytical and numerical derivatives signifies deviation from radial flow.

Fig. 1 displays the performance of an injector well in a geothermal reservoir.

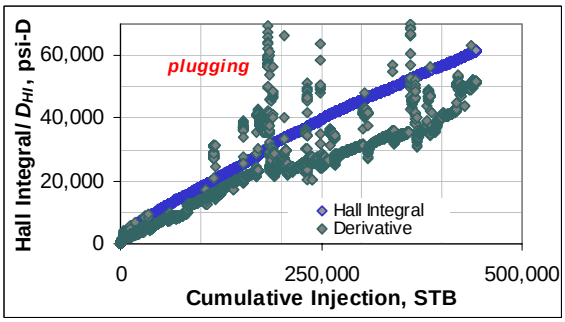

Figure 1. Modified Hall plot of an injector in a geothermal reservoir.

The diagnostic plot shows multiple cycles of fracturing and plugging. Shortly after the initiation of injection, fracturing takes place. The constant downward separation distance between derivative curve and Hall integral implies that injectivity is retained. At the final stages the well begins to show signs of plugging again preceded by large multiple fracturing events.

NUMERICAL MODEL

To simulate the interaction between dilated fracture and fluid flow in this study, we utilized a Chevron proprietary geomechanical reservoir simulator, GMRS®, which fully couples geomechanics and reservoir fluid flow. While tensile fracturing occurs quickly (within a few minutes to several hours), dilatant of fracture takes much longer (months).

To model injectivity response by long term cold water injection, we set a fracture plane that passes through both the injector and producer as shown in Fig. 2.

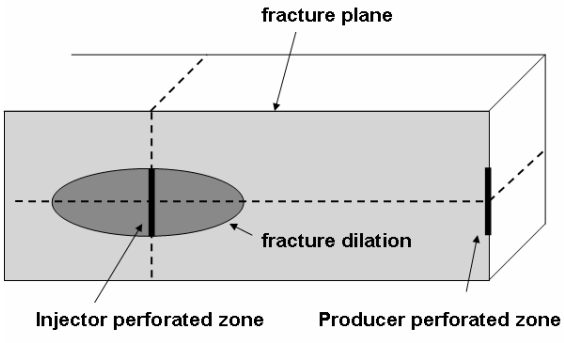

Figure 2. Schematic of fracture propagation.

We set a separate grid system for the fracture so that the conductivity of the cells that contain the fracture can be explicitly solved. However, due to the current simulator limitations, the fracture plane is limited to

2D and its orientation needs to be prescribed by users. In this study, the fracture plane is located at y=0.

Base Case Description

As a base case for our study, a realistic situation was prepared. Fig. 3 shows a schematic of the physical domain.

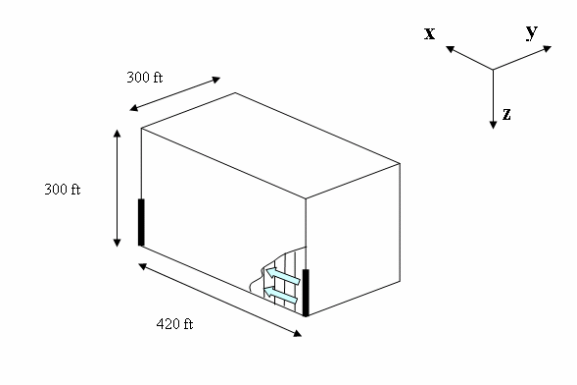

Figure 3.Physical domain of the model.

This is ¼th of the domain depicted in Fig. 1 and cold water is injected from the injector at one end to improve the injectivity of this well by dilating the existing fracture. No flow boundaries are considered except for the y=300 ft plane where constant pressure is set. We set all vertical displacements zero. Also at x boundaries (x = 0 and 420 ft) and y boundaries (y = 0 and 300 ft), all nodes are fixed.

The geomechanical, reservoir and well parameters used in this study are listed in Tables 1, 2, and 3 respectively.

Table 1 Geomechanical parameters.

Young's modulus		psi	8.57E+06
Poisson's ratio			0.25
Biot's constant			1
Thermal Expansion Coeff.		1/F	9.57E-06
Density		gm/cc	2.65
Stress	vertical	psi	4200
	maximum	psi	4000
	minimum	psi	2500

Table 2 Reservoir parameters

Reservoir	pressure	psi	1550
	temperature	F	350
Permeability		md	0.01
Porosity			0.1

Table 3 Well parameters

BHP	producer	psi	1550
	injector	psi	3250
Simulation time		day	100

A 3D grid system comprising 46x15x15 cells originating at (0 ft, 0 ft, 4200 ft) was utilized. An injector is located from (0 ft, 0 ft, 4250) to (0 ft, 0 ft, 4500 ft), and a producer is located from (420 ft, 0 ft, 4250) to (420 ft, 0 ft, 4500 ft). The grid system is shown in Fig. 4.

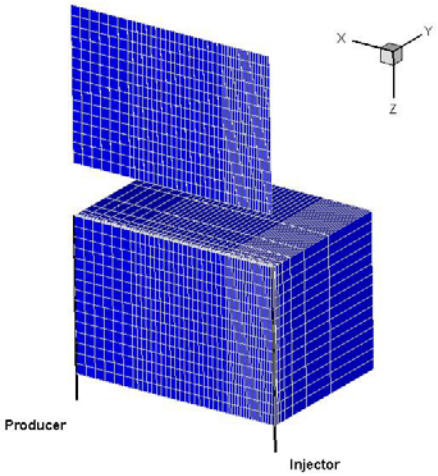

Figure 4 Grid system for reservoir and fracture.

The fracture grid is displayed above the reservoir system for visualization purpose. In the computation process, solutions are obtained by coupling these systems. In the following examples, we consider the fracture width to be 2 cells uniformly. Since the matrix has little permeability, the fracture will be the only flow path and injectivity will be increased by dilation of the existing fracture. Fig. 5 shows the temperature profiles of both fracture and matrix at 60 days.

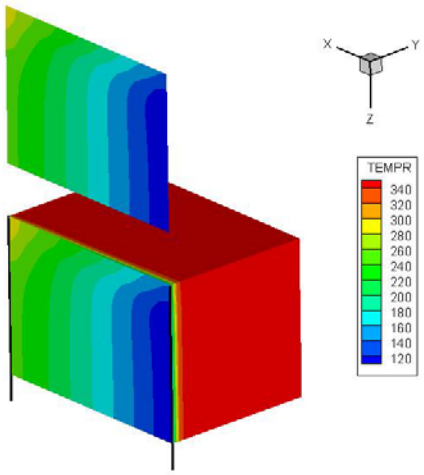

Figure 5 Temperature profiles at 60 days.

From the figure, we can see the cold temperature front moves fast in the fracture. Into the formation, heat is transferred by both convection and

conduction. Because of the low permeability of the rock, conduction is dominant. Therefore the heat transfer to the matrix is very slow.

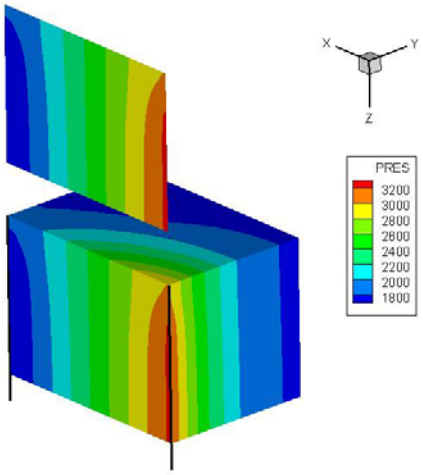

Figure 6 Pressure profiles at 60 days.

Fig. 6 shows the pressure profiles of fracture and matrix at 60 days. Mass transfer between fracture plane and matrix is computed based on the pressure difference of the systems. We can see from the figure that pore pressure in the matrix built up from its initial reservoir pressure (1550 psi) near the injector. When looking at the stress profile of the matrix in the y-direction (minimum direction) at 60 days (Fig. 7), high stress occurs where the pressures are building up. Meanwhile, in the cold thermal front region (see Fig. 5), we can observe that the stresses are being reduced.

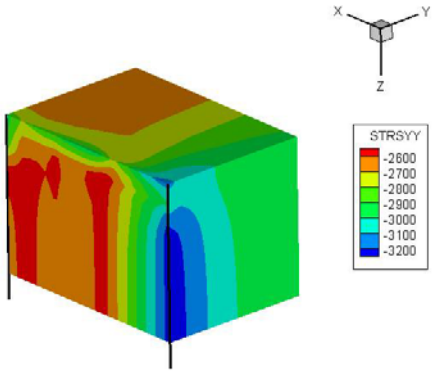

Figure 7 Stress profile at 60 days

Fig. 8 shows the dilated fracture half width and length with time. As the fracture length (x-direction) follows the fracture grid system as shown in Fig. 4, its dilation will follow the size of grid block in x-direction. The fracture is stimulated rapidly after the start of injection and begins to slowly close as pore pressure gets built up. In later time, the fracture starts to dilate again since the matrix is cooled with time and the stresses are reduced (thermoelastic effect becomes significant).

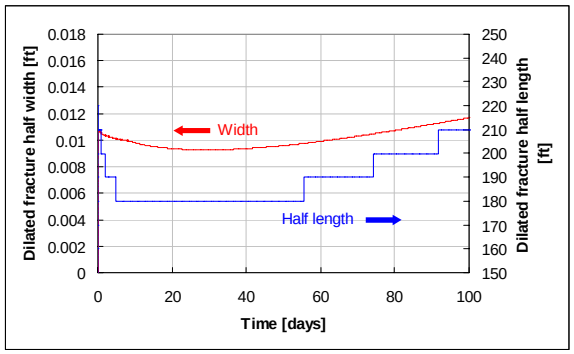

Figure 8 Dilated fracture half width and length.

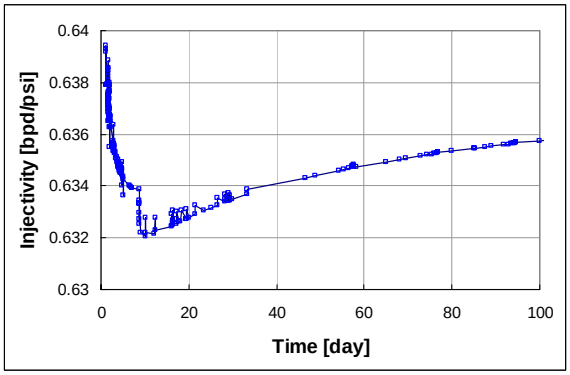

Figure 9 Water injectivity history.

Water injection rate history is shown in Fig. 9. Injection rate shows a rapid drop in early time and then shows steady improvement. In field operation, it is hard to decide if fracturing is occurring or if the formation is being plugged. As described above, we could identify the fracture (negative skin) propagation with a reformulated Hall plot method. Fig. 10 shows the reformulated Hall plot of the base case.

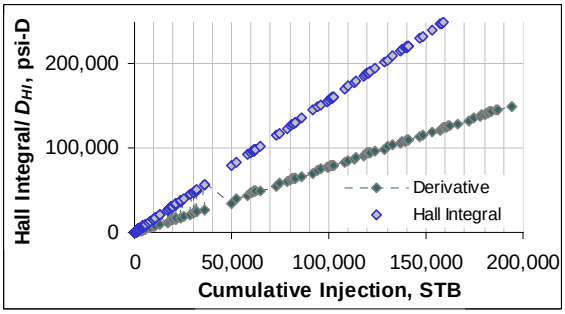

Figure 10 Reformulated Hall plot for base case.

From the figure, we can see the fracture continuously growing and this is consistent with the simulation results as depicted in Fig. 9.

STIMULATION DESIGNS

We seek to achieve the maximum injector performance under normal operating conditions where different types of injection fluids and zonal isolation tools are not readily available.

First, cases with various injection temperatures and pressures were conducted to infer the sensitivity of injector performance to these conditions. Then a well shut-in case was run. In field operations, injectivity improvements have been observed after the shut-in of the well. Possible explanations for this phenomenon could be the effect of the cycling pressure at the injector. To address these issues, cases with temperature and pressure cycles were run. The injectivity improvement will be evaluated by computing the injectivity index, which is defined as

$$II = \frac{i_w}{\left(p_{wf} - p_e\right)} \qquad (4)$$

Injection Temperature

As the formation gets cooled, stresses are reduced. The reduction in the stress would be proportional to the temperature change. We simulate the cases with the injection temperature of 80 ^{o}F and 120 ^{o}F. Fig. 11 shows the dilated fracture half width with time.

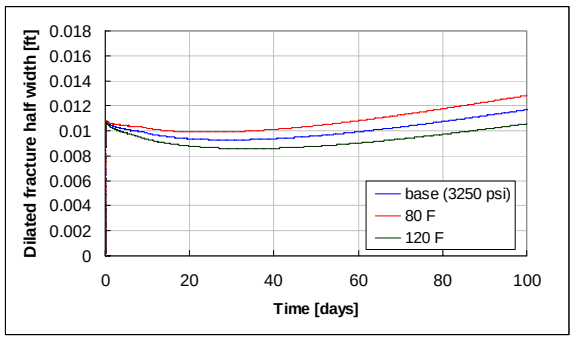

Figure 11 Fracture half width dilation (various temperature).

From the fracture propagation history, we can see the starting fracture widths are identical. With injection of warmer 120 ^{o}F water, the fracture width is not as large at a given time as indicated in the base case (lower curve). At 80 ^{o}F the fracture width is larger than the base case. Injectivities of each cases are plotted in Fig. 12.

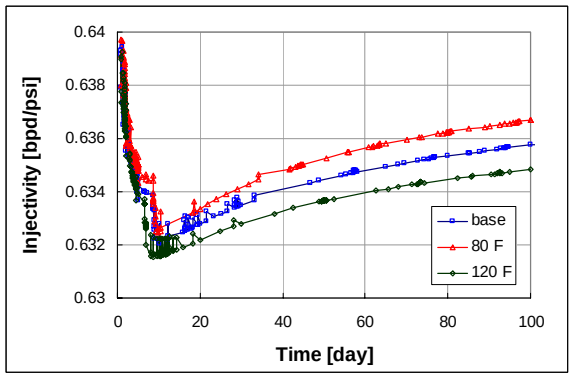

Figure 12 Water injectivity history (various temperature).

Separation from the base case begins after the initial injectivity drop and the separation keeps growing as the water injection goes on. As can be seen from the examples, injection temperature has long term effects.

Injection Pressure

To create a large surface area by dilatant fracturing, increasing the injection pressure would be the most effective solution. However, due to operation restrictions, increasing injection pressure is often not possible. In this example, we simulate the cases of BHP 3000 psi and 3500 psi along with the 3250 psi base case to see the effects of injection pressure. Fig. 13 shows the dilated fracture half widths with time.

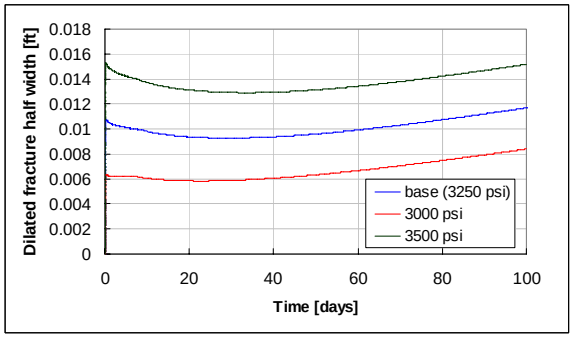

Figure 13 Fracture half width dilation (various pressure).

As expected, the fracture will be dilated more with the higher injection pressure. In all the cases, they follow very similar trends. The injectivities are shown in Fig. 14.

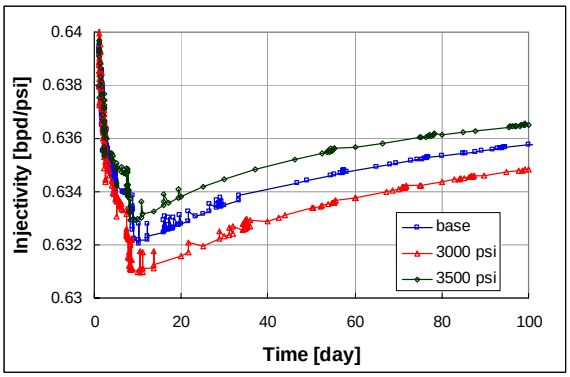

Figure 14 Water injectivity history (various pressure).

Increasing the injection pressure has similar effects to cooling injection temperature. However, while cooler injection case shows constant separation from the warmer injection temperature case, the injectivity differences between different pressures stay almost the same.

Shut-in

In fields, the injectivity has been observed to improve after shut-in. In this example, we examine the effect of well shut-in. All the other parameters are the same as the base case. We shut the well in for one day after 50 days of stimulation and restart the injection at 51 days. Figs. 15 and 16 show the injectivity and the dilated fracture half width of the shut-in case compared with the base cases.

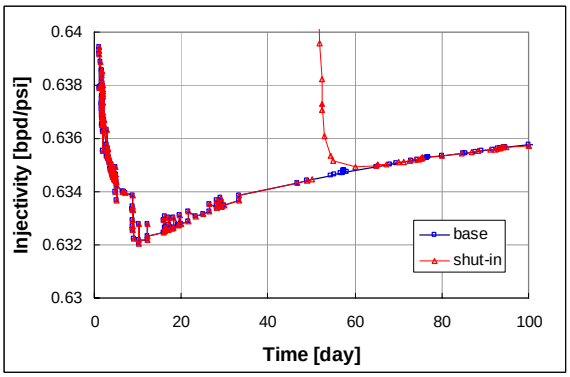

Figure 15 Water injectivity history (shut-in).

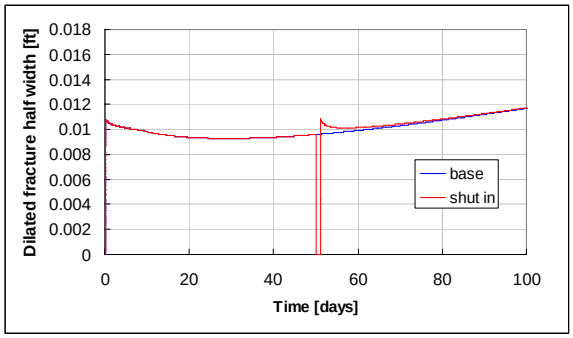

Figure 16 Fracture half width dilation (shut-in).

After the well was re-opened, the injectivity shows a big spike and the injectivity overrides the base case for about 10 days after re-opening the well. Also the dilated fracture width history shows that fracture dilates more than before the shut-in and it eventually goes back to the base case level. Fig. 17 shows pressure and stress profiles before (at 50 days) and after the shut-in (at 60 days). The pressure in the fracture is temporally reduced and stress is lowered as well. This temporal reduction in stress allowed the fracture to dilate more than the pre-shut-in level.

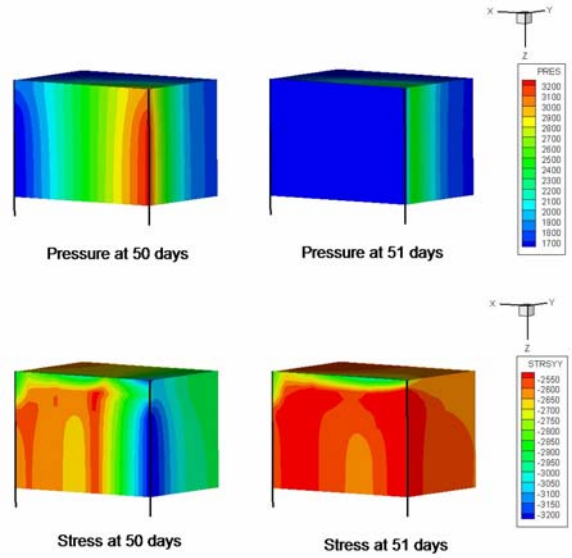

Figure 17 Pressure and stress profiles before and after well shut-in.

Pressure/Temperature Cycling

In this section, we will go through the cycling of injection rate (BHP) and injection temperature to see if we will obtain any additional stimulation compared to holding them constant.

First, we simulated a pressure cycling example. The pressure cycling scheme follows the schedule shown

in Table 4 and the resulting dilated fracture half width history is plotted in Fig. 18.

Table 4 Cycling BHP

Time (days)	BHP (psi)
0-50	3250
50-60	3000
60-70	3500
70-100	3250

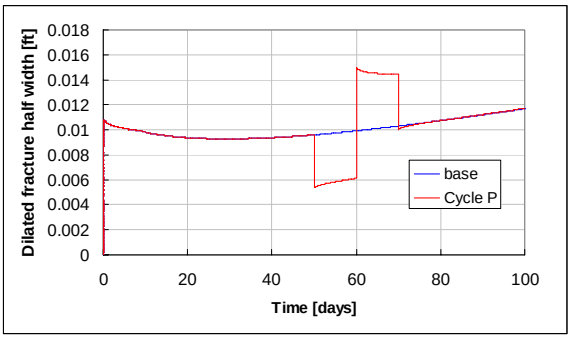

Figure 18 Fracture half width dilation (cycle pressure).

Although fracture dilation seems very sensitive to the BHP change, after the pressure cycle occurs, the fracture width returns to nearly the same value as the base case. This plot shows that lowering the pressure immediately leads to closing a fracture. Increasing the pressure can recover the fracture dilation. However, the fracture dilation neither gains nor loses at the end. The injectivity history is shown in Fig. 19 with the case of BHP 3500 psi.

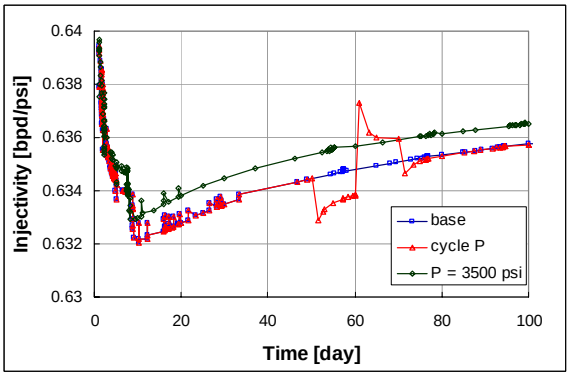

Figure 19 Water injectivity history (cycle pressure).

Similarly, temporary changes to injectivity are seen as the injection pressure is being changed. The injection rate for the cycling pressure case exceeds the base case, but only temporarily. However, the injectivity converges to that of the base case, which injects with the constant pressure continuously, resulting in a lower injectivity than a constant BHP of 3500 psi.

As a last example, we investigate the effect of cycling injection temperature. The injection temperature cycle for this example was performed as listed in Table 5.

Table 5 Cycling injection temp

Time (days)	Injection temp (^{o}F)
0-50	100
50-60	120
60-70	80
70-100	100

The intention of the last example is induce a thermal drawdown artificially by cycling warm and cold water. The dilated fracture half width is shown in Fig. 20 and the injectivity history is plotted with the case of 80 ^{o}F injection temperature and shown in Fig. 21.

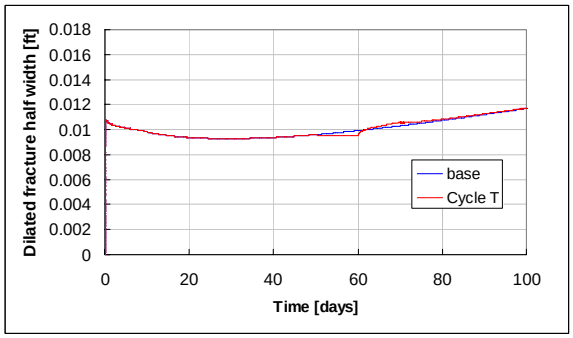

Figure 20 Fracture half width dilation (cycle temperature).

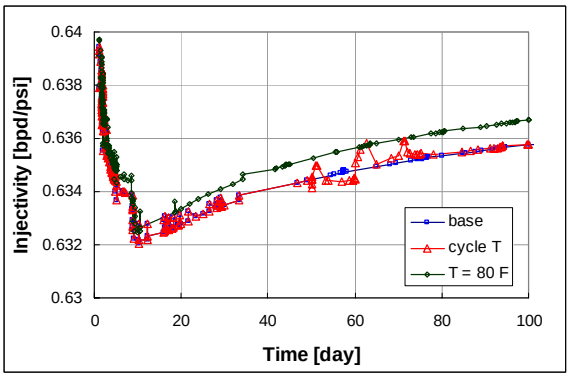

Figure 21 Water injectivity history (cycle temperature).

The fracture dilation shows very subtle changes. The water injectivity also depicts small effects. Although it indicates some improvements in the injectivity after switching injection temperature, we would achieve better water injectivity if the injection temperature is cool in the first place.

Optimal Injection Scheme

From the various examples above, we have observed that higher pressure and colder injection temperature will result in better injectivity. Also, by shutting in a well, we see injectivity spike along with the fracture dilation, but the effect is temporary. Pressure or temperature cycling does have some effects on the injectivities, but would not have additional benefits to injecting with high pressure or cool temperature as available.

Therefore we should operate water injection under as high pressure and cool injection temperature as we can to take a full advantage of long term cold water injection. Given injection pumps and facility capacity, additional injectivity improvement may be obtained through shutting in a well.

For an optimal water injection scheme, we examined the effects of duration and frequency of well shut-in. First, various durations of well shut-in were studied. Figs. 22 and 23 show water injectivity and dilated half fracture width with shut-in duration of 1, 2, 5, and 10 days.

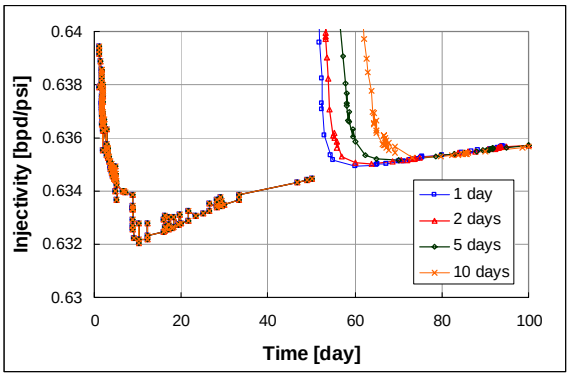

Figure 22 Water injectivity history (shut-in duration).

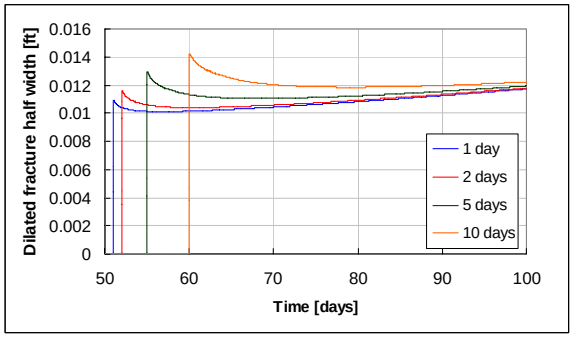

Figure 23 Fracture half width dilation (shut-in duration)

The injectivities show an instant jump after the shut-in, but in all cases, it lasts for about 10 days, similar to 1 day shut-in duration case. Although the dilated fracture width indicates longer term effect in longer shut-in duration, the effects are still transient and last about 100 days.

Secondly, we investigated the effects of shut-in frequency. We compared results from shut-in frequency of 1 (at 50 days), 2 (at 50 and 75 days), 5 (at 50, 60, 70, 80, and 90 days), and 10 (at 55, 60, 65, 70, 75, 80, 85, 90, and 95 days). The injectivity and fracture width dilation histories are shown in Figs. 24 and 25.

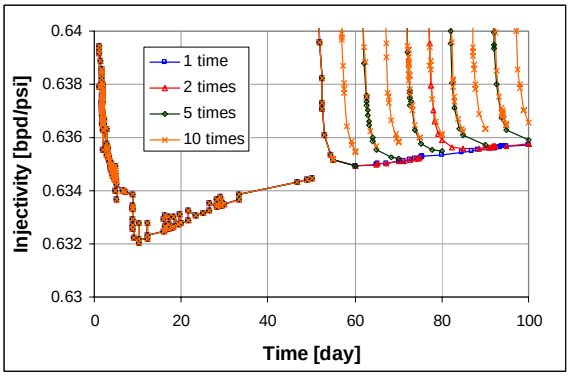

Figure 24 Water injectivity history (shut-in frequency).

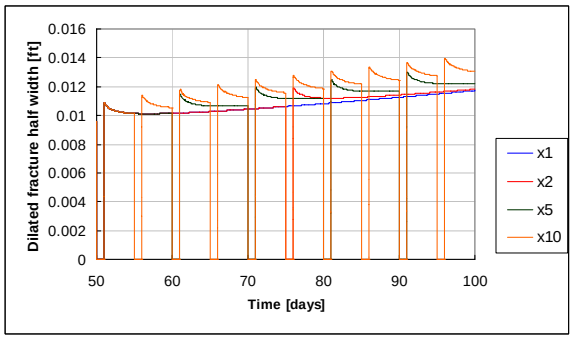

Figure 25 Fracture half width dilation (shut-in duration)

The injectivity history similarly shows a spike after shut-ins and with the frequency of 10, it shows an increasing trend. The fracture width dilation history also shows an increasing trend in the width and at 100 days, the fracture half width dilation is improved by 30% (0.03 ft) even though the total shut-in duration is same as the previous 10 days shut-in example.

SUMMARY AND CONCLUSIONS

A conceptual sector model was developed to study the optimal water injection stimulation design. A number of operational conditions were simulated to understand their effects on the injectivity and fracture

dilation. As the model contains only a single fracture in the domain, it may no represent a whole complex naturally fractured system though. The following conclusions drawn from this study should apply in general:

1. The higher the injection pressure and the cooler injection temperature, the more the fracture dilates.
2. Cycling pressure or temperature improves injectivity but it does not outperform the injection operation with the highest pressure or coolest temperature all the way through.
3. Well shut-in stimulates fracture dilation temporally. Periodic well shut-in can constantly improve injectivity and shut-in duration shows less sensitivity to the injectivity performance.

ACKNOWLEDGEMENTS

The authors wish to extent their sincerest gratitude to the management of Chevron Geothermal and Power and Chevron ETC Houston for their kind permission to publish this work.

NOMENCLATURE

B	formation volume factor, RB/STB
h	formation thickness, ft
II	injectivity index, STB/psi
i_w	injection rate, STB/D
k	permeability, md
p_{wf}	bottomhole pressure, psi
r_e	water bank radius, ft
s^*	pseudo skin, dimensionless
W_i	cumulative water injection, STB
μ	fluid viscosity, cp

REFERENCES

Hall, H.N., "How to Analyze Waterflood Injection Well Performance," *World Oil* (October, 1963), 128-130.

Izgec, B., and Kabir, C.S., "Real-Time Performance Analysis of Water-Injection Wells," paper SPE 109876, presented at the 2007 SPE Annual Technical Conference and Exhibition, Anaheim, CA, 11-14 November.

Kappelmeyer, O., and Jung, R., "HDR Experiments at Falkenberg/Bavaria," *Geothermics* (May, 1986), 375-392.

Mahajan, M. Pasikki, R., Gilmore, T., Riedel, K., and Steinback, S., "Successes Achieved in Acidizing of Geothermal Wells in Indonesia", paper SPE 100996, presented at the 2006 SPE Asia Pacific Oil & Gas Conference and Exhibition, Adelaide, Australia, 11 – 13 September.

Pasikki, R.G., and Gilmore, T.G., "Coiled Tubing Acid Stimulation: The Case of Awi 8-7 Production Well in Salak Geothermal Field, Indonesia," presented at the 31st Workshop on Geothermal Reservoir Engineering, Stanford, CA, 30, January – 1, February.

Smith, M. C., Aamodt, R.L., Potter, R.M., and Brown, D.W., "Man-made Geothermal Reservoirs," Proceedings UN Geothermal Symposium, 1975

Tenma, N. *et al.*, "Productivity Changes in the Multi-Reservoir System at the Hijiori HDR Test Site during the Long-Term Circulation Test," *Geothermal Resources Council* (September, 2002), 261-266.